City, University of London Institutional Repository

PARAMETRIC STUDY AND FLOW CHARACTERISTICS OF A NEW DUCT FOR DUCTED WIND TURBINES SYSTEM USING ANALYTICAL HIERARCHY PROCESS: NUMERICAL & EXPERIMENTAL STUDY

Javad Taghinezhad[1]*, Reza Alimardani[1], Mehran Masdari[2], Hossein Mosazadeh[1]

[1] Department of Biosystem Engineering, Faculty of Engineering & Technology, University of Tehran, PO Box 4111, Tehran 13679-47193, IRAN

[2] Faculty of New Science and Technology, University of Tehran, Tehran, IRAN

ARTICLE INFO

Abstract

This paper aims to study aerodynamic modeling and optimization of the ducts to increase the power efficiency of ducted wind turbines. We design ducted wind turbines based on the features used to determine the sizes and indices of wind tunnels. Many researchers used analytical and numerical methods to select the optimized duct. This study evaluates the effect of design parameters, such as nozzle length, contraction ratio, and outlet diameter, on multiple responses. By applying the analytical hierarchy process (AHP), we find the best design of a duct optimizing the multi-criteria responses. A duct prototype is fabricated to validate the optimal design, and experimental analyses are conducted based on the fabricated duct. A measurement system estimates the pressure distribution in the inlet contraction section; then, a hot-wire sensor investigates wind speed and the flow turbulence in the throat section. A good correlation between calculated data and measured values was found during the estimation of pressure distribution along the inlet contraction wall. Investigation of flow turbulence in the throat section indicates velocity in the duct throat can increase from 2.6 to 2.9 times related to the free flow velocity at different working speeds. Spectral analysis of the flow signal inside the duct shows two peaks in a frequency lower than 32 *Hz* related to wind tunnel vibration and Gartler vortex. Then, the flow disturbances will not significantly impact the performance of the wind turbine placed inside the duct throat.

Keywords: Renewable Energy, Ducted Wind Turbines, Accelerating Wind, CFD Analysis, AHP, Spectral Analysis

Nomenclature	
ρ	Density
θ_e	Expanding angle of the diffuser

θ_w	Flow streamlines angle with Z axis
θ_v	Flow streamlines angle with Y-axis
C_p	Pressure Coefficient
D_e	The diameter of the exit plan at inlet contraction
D_i	The diameter of the inlet plan at inlet contraction
L	Length of inlet contraction
m	Meter
P	Static Pressure
PSD	Power spectrum distribution
P_∞	Free Stream Pressure
R_1	The radius of the inlet plan at the diffuser
R_2	The radius of the outlet plan at the diffuser
Re	Reynolds number.
s	Second
x_m	The axial location of the match point
u, v, w	axial components of the velocity
U	Flow velocity along the axis of the turbine
$\tilde{u}$	Non-uniformity of the maximum flow
u_{avr}	Mean axial velocity at the plan
V_1	The velocity of the inlet flow to the diffuser
V_2	The velocity of the outlet flow of the diffuser
W	Weight of alternatives
W_t	The final weight of each criterion

1   Introduction

Wind energy is one of the most reliable forms of energy, and increasing the efficiency of the wind turbine helps generate cost-effective power [1–3]. Even though conventional wind turbines already operate worldwide, they have disadvantages, such as high installation costs, restrictions on wind farm locations, and complex energy production technology [4]. Accordingly, designing a wind turbine with fewer limitations, such as ducted wind turbines (DWT), has gained more attention these days. DWTs can be installed in some areas with relatively lower wind speed as they can utilize the energy in the wind more effectively while focusing on energy extraction and acceleration. Even with lower wind speed available, the electricity generation of DWTs is comparable to that of conventional wind turbines installed at locations where strong wind is available. Hence, it is possible to generate electricity over a wide range of regions with lower average wind speeds than conventional turbines. With less restrictions on turbine locations, DWTs can be placed close to demand areas. Such proximity can reduce the cost of power transmission and the energy losses in electricity distribution and transmission, which accounted for more than 6% of total electricity generation between 2002 and 2008, according to the US Energy Information Administration (EIA) [5]. Since wind energy sources widely depend on geographic location, DWTs have focused on converting energy near consumption sites, eliminating high-cost transmission lines, and reducing transmission losses[6].

Invelox, Zena, and Airborn are the most popular DWTs which are under development by researchers. In all types of these turbines, a general wind turbine is located in a convergent-

divergent duct [7]. Allaei [8] introduced Invelox, including a tower that captures wind energy and a convergent-divergent section to locate a wind turbine and transmit wind energy to electricity. The follow-up researches from the same author [9, 10] focused on the structure of tower and wind capturing units and presented there is about two times increment in wind speed in Invelox related to the free stream. Anbarsooz et al. [11, 12] presented another study on Invelox wind turbines performance. They showed that velocity increment in Invelox could reach up to 1.9 times free-stream wind. Some preliminary studies have been done on the effect of diffusers and contraction sections on wind turbines [13–17]. The fundamental principle in DWTs is to increase the energy density in a rotor relative to the same wind in free flow [18]. DWTs can typically produce more power than a fixed-diameter rotor; in other words, DWTs can generate more power from fixed areas than conventional turbines [4, 9, 10]. Economically, by reducing the size and cost of the rotor, DWTs can save more [19, 20]. Masukume [21] reported that the levelized unit cost of energy of the ducted wind turbine is USD 0.26/kWh compared to USD 0.30/kWh of the conventional wind turbine. To get more details about power efficiency and design details, Taghinezhad [22] reviews other researchers' studies on DWTs.

In this regard, there isn't any focus on duct wall design and its effect on the output power of DTWs in previous research; this paper introduced a design method for DWTs using the features used to determine the sizes and indices of wind tunnels. Then the main aim of this work is to optimize the dimensions of the duct enclosing the wind turbine and improve the duct performance by using a new method to design the duct wall. Therefore, a parametric study of the duct is needed; this study investigates the flow stream characteristics within many ducts with defined geometries and different parameters using CFD simulations. The effect of increasing the contraction ratio and length of each part is investigated separately, and parameterized design is presented to clearly show the effective geometrical range of a simple duct for commercial small wind turbines.

Several ducts were simulated to introduce the optimized duct. Each duct had its performance for difference parameters defined to evaluate the ducts. We need a multi-criteria analysis method to select the best duct. Then, a multi-criteria analysis (MCA) framework is used to analyze and compare calculated parameters from CFD analysis in terms of relevant criteria, including quantitative and qualitative ones. We apply the Analytic Hierarchical Process (AHP) to the calculated data to select, combine and weight the different criteria to more reliable MCA outcomes. The analysis has been done for different calculated parameters of the designed duct. The AHP is considered a standard and efficient method applicable to decision-making issues with complex hierarchies. Applications of the AHP are found in different wind

energy areas, from selecting wind farm sites to energy transfer systems. Solangi [23] mentioned that it is substantial to prioritize possible sites to build new wind power plants. It is a multifaceted decision process; then, they used the AHP method to prioritize sites in the southeastern region of Pakistan. Dinmohammadi and Shafiee [24] used the AHP method to evaluate various technology transfer solutions to design and manufacture wind turbines. Four main criteria and nine sub-criteria were defined, and the weights of the criteria and sub-criteria were calculated using AHP. Konstantinos [25] used the AHP for selecting wind farm installation locations in Greece. They design a Decision Support System (DSS) that can encapsulate all the parameters affecting the installation of a wind farm to minimize setbacks and maximize the produced energy. AHP is a scientific method to support researchers in making effective decisions concerning several inconsistent criteria and provides decision-makers with some tools to solve a complex issue with different points of view that are taken into account. Because of the broad usage of AHP in research, we used AHP as an MCA method to determine the best operational sections for the designed duct.

This paper is structured as follows, in Section 2, the method to design the duct's different parts is presented. The duct is divided into three sections, and the simulation method for each section is described. Then required parameters to analyze the designed duct introduced. In section 3, the CFD approach implemented in the ANSYS CFX software is explained in detail.In section 4; examination method in experimental tests described required apparatus and setup arrangement in wind tunnel tests presented. In section 5 AHP method introduced to select the best design output among different models. In section 6 spectral analysis method is described to measure the energy level of the output signal from wind flow. In section 7, the results of simulations presented and the best duct selected, then the results from simulations compared with experimental tests to confirm CFD analysis. After that, flow turbulence and spectral analysis results are presented and discussed.

2 Design of the Duct

The duct design was performed based on various wind tunnel components in three sections of the duct. As mentioned by researchers in optimization of the wind tunnels [26], the design requirements that the designed duct shall meet are as follows:

1) The duct shall have a suitable inlet for receiving wind flow.
2) The duct shall generate the maximum possible wind acceleration and speed in a limited space.

3) The duct shall have a suitable location for installing the turbine and converting wind energy to mechanical energy.

4) The duct shall have a section to recovery the dynamic wind pressure after energy absorption.

5) The duct assembly shall be designed to prevent critical boundary layer/ flow separation at the contraction section and maximize the available power at the duct throat section (turbine position).

The objective of this study is to design the duct wall. It covered three sections, including inlet, throat, and diffuser sections. The duct is divided into three sections to consider the parametric study on each part. As shown in Figure 1, a sample for ducted wind turbine systems, the inlet section was designed based on a method introduced by Morel [27]. The throat section was considered a location for installing the wind turbine. The outlet section included recovering the wake flow outcome from the throat section and delivering flow to the environment.
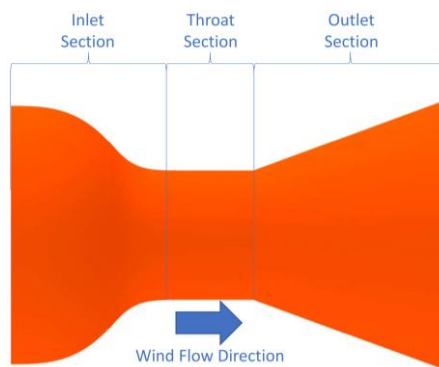

Figure 1 - Overall Structure of the ducted wind turbine systems

2.1 Design of Contraction Section

The inlet contraction design is essential for retaining good flow quality in the throat section [26]. The size and shape of the inlet contraction also determine the level of turbulence intensity in the throat section [28]. The inlet contraction length should be as small as possible to minimize boundary layer growth and fabrication costs. However, this section should be long enough to prevent a large reverse gradient pressure along the wall, leading to the flow separation [29, 30]. The separation of flow occurs in places with a pressure gradient, so the inlet contraction should be designed to minimize the occasion of separation.

To design the inlet contraction, we use the third-order polynomial matching method with an eighth-order polynomial, proposed by Morel [27] and used by other researchers [31–33] for the same purpose. The schematic of the contraction polynomial used at the inlet contraction

is shown in Figure 2. The D_i is inlet diameter, D_e is outlet diameter, L is the total length of contraction section, and x_m is the location of match point.
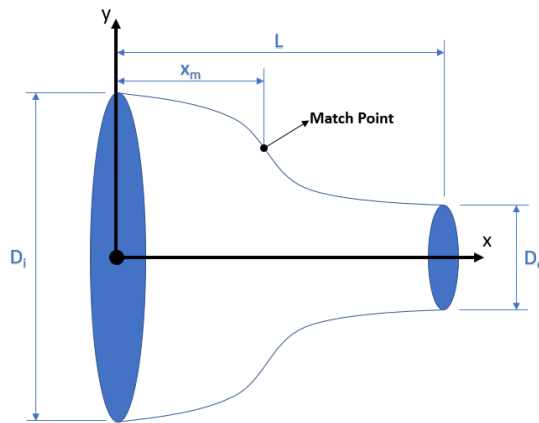

Figure 2- Schematic of inlet contraction section polynomials

To design the inlet contraction section, a set of parameters including contraction ratio, the diameter of the inlet section, and length of the contraction section were selected. For making the wall curve, the match point of polynomials was selected on $x_m/L = 0.5$ based on the results reported by Mathew [26]. For the other parameters, three different diameters specified for D_e (0.13, 0.145 & 0.16 m) regarding blockage ratio shall not exceed 20% of wind tunnel test section. Three lengths for the contraction section were selected 0.25, 0.75 & 1.5 times of D_e; based on Sukumar research [34], the optimized length of the contraction section is between 0.25 to 1.25 times of D_e, and contraction ratios were determined 2, 3, 4, 6 and 8 while blockage ratio not exceeding than 20% [35]. Figure 3 shows the twenty-seven curves simulated for the inlet contraction wall. X indicates the length of the duct from the center point in the section of the duct, and Y shows the distance of the duct wall from the central axis of the designed ducts, same as shown in Figure 2. These inlet contractions were modeled in Ansys CFX software to analyze the flow characterization in each model.
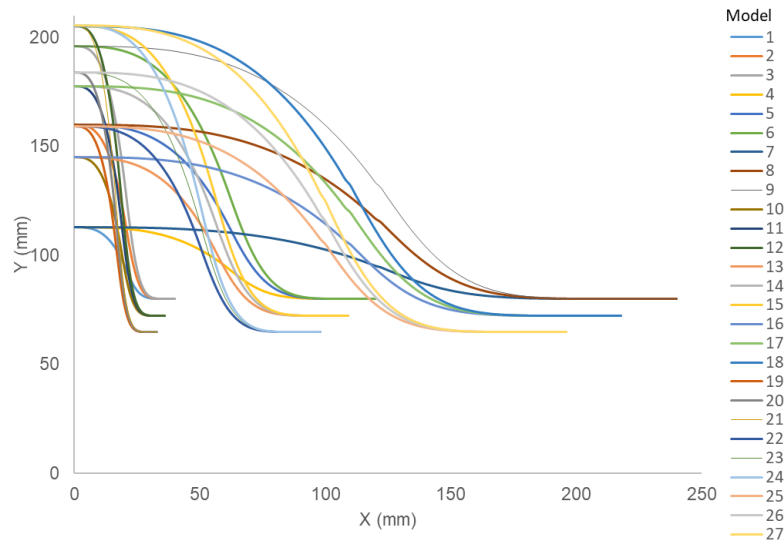
Figure 3 - Designed curve for inlet contraction wall

2.2 Design of Throat

Placing a wind turbine inside the ducts requires a fixed area throat because the contraction in the inlet section results in an unsteady flow before wind reaches the turbine; this causes the flow separation behind the turbine. With the flow stream inside the duct length, its energy drops down. To prevent these droplets, the length of the throat should be as small as possible. However, the length of the throat should be long enough to allow flow to extend before reaching the wind turbine [26, 34]. As we know, the diameter of the throat section is equal to the outlet diameter of the inlet section (D_e); therefore, to select the optimum length of the duct throat in this study, three values of 0.25, 0.75, and 1.5 times the diameter of the duct throat were used to study the optimum length of the duct throat.

2.3 Design of Diffuser

The purpose of the diffuser is to recover the static pressure drop caused by inlet contraction and throat sections [36]. So, it is better to reduce wind speed in the diffuser section with minimum possible energy loss. In general, it is advisable to reduce the wind speed in the shortest possible distance while there is no flow separation. This point improves efficiency and reduces fabricating costs by reducing the size of the diffuser section. The diffuser is sensitive to design errors that may cause partial or steady separation. Its area should be more extensive in the flow direction to prevent separation along with the diffuser [26].

Pressure recovery in the diffuser depends on the mass flow, density, and section area of the diffuser inlet and outlet and is independent of the diffuser's shape. The diffuser was modeled as a simple cone with two parameters of expanding angle (Θ_e) and expanding ratio (A_2/A_1). Values 6, 9, and 12 degrees for Θ_e and 5%, 10%, and 15% expanding ratios were

selected for designed diffusers (Figure 4). V_1 is the diffuser's input wind flow speed, while V_2 is the output wind flow speed through the diffuser. R_1 and R_2 are the inlet and outlet radius of the diffuser, respectively.
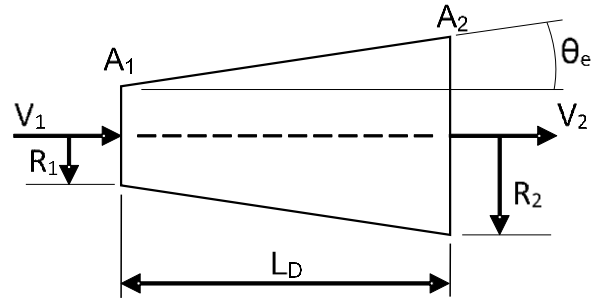

Figure 4 - Schematic of the diffuser parameters

2.4 Measured variables in the designed duct

Flow stream quality at the throat section can be evaluated by three parameters, θ_w, θ_v, $\tilde{u}$, and separation, which form the cost function for optimization studies.

θ_w is the angle the flow streamline makes with the z-axis due to the curvature of the wall, where the z axis is perpendicular to the x and y axes is represented by the following equation:

$$\theta_w = tan^{-1}\frac{w}{u_{avr}} \qquad (1)$$

where w (m/s) is the velocity in the z-direction at the output of the inlet contraction section and u_{avr} is the mean axial velocity at the output. The best duct should present the minimum possible values for θ_w. Similarly, θ_v is the angle that the flow streamline makes with the y-axis and is calculated by the following formula:

$$\theta_v = tan^{-1}\frac{v}{u_{avr}} \qquad (2)$$

where v (m/s) is the velocity in the y-direction at the output of the inlet contraction section, the best duct should present the minimum possible values for θ_v. The non-uniformity of the maximum flow in the inlet contraction section is calculated as follows:

$$\tilde{u} = \frac{u_{max} - u_{min}}{u_{avr}} \qquad (3)$$

where u_{max} and u_{min} are the minimum and maximum values of velocity in x-direction on the output section of the inlet contraction, respectively, the best duct should present the minimum possible values for $\tilde{u}$.

The Stratford criterion [37] was used to investigate the separation of the boundary layer within the duct. This criterion was previously used by Morel [27] and was a well-known

analytical tool to investigate separation at the boundary layer. The pressure coefficient was examined along the duct wall to investigate the separation in the duct. It must be ensured that these pressure coefficient values are lower than those predicted by the Stratford criterion, which indicates the separation range. For the designed ducts, no separation in the duct wall is allowed. Then, in comparison to the other criteria, this parameter has a higher weight in the outcomes. The mathematical form of the Stratford Criterion is as follows:

$$c_p \left(\frac{x \, dc_p}{dx} \right)^{0.5} = 0.39 \left(10^{-6} \, Re \right)^{0.1} \qquad \textbf{(4)}$$

where x is the axial distance along the duct, c_p is the pressure coefficient, and Re is the Reynolds number.

3   CFD Simulation

Using the ANSYS CFX software, a mathematical model was built to simulate the flow inside the proposed ducts. The ambient and wind flow temperatures were assumed to be constant at 300K in the design assumptions. The air was assumed a non-compressible Newtonian fluid with a density of 1.225 kg/m^3 and a pressure of 1 atmosphere as the system's intake fluid. Figure 5 shows the optimized computational domain for attaining the optimal dimensions of the final domain and solving the issue regardless of the domain dimensions. The domains were modeled as a cube, with the following values proposed in Pinto and Giahi's investigations [38, 39].
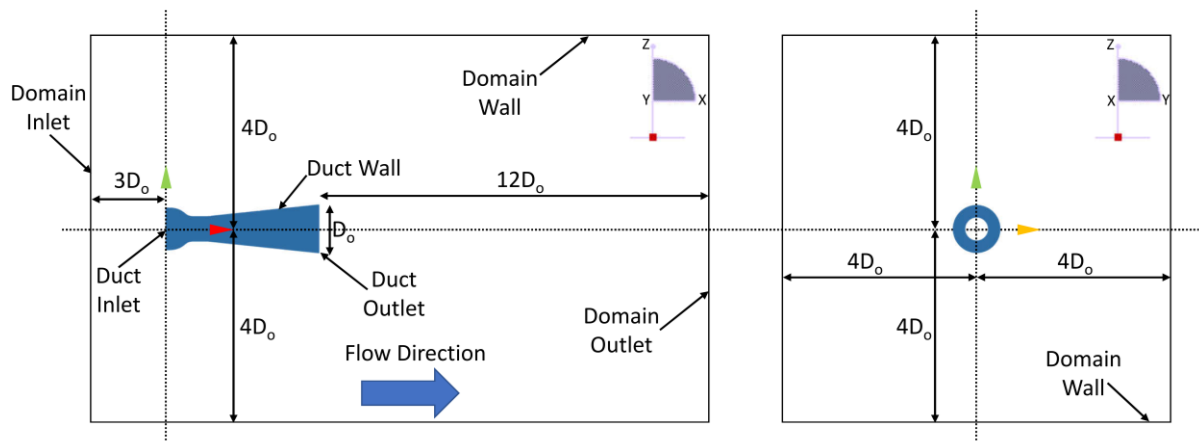
Figure 5 – A sample duct domain with its boundary conditions.

The aerodynamic turbulence of the flow through the duct was predicted using the Shear Stress Turbulence (SST) technique. Due to its great capacity to examine various factor impacts on flow stream transfer, such as free-stream flow turbulence and pressure gradient, the SST technique can properly investigate the boundary layer [40]. RANS equations, which combine continuity and Navier-Stokes functions with the finite volume technique assumption,

were used for numerical modeling [41, 42]. The upwind Scheme approach was employed to regulate and decrease numerical computation errors. The inlet, outlet, walls, and interfaces are all boundary conditions in this domain. A No-Slip wall was established as a boundary condition in the walls. It should be noted that the flow in this study is always Subsonic due to the low-speed wind. In the free stream flow range, the turbulent flow of the input wind to the computational domain was assumed to have a speed of 10 m/s and an intensity of 5%. The General Grid Interface (GGI) was used to link the duct input and output to free streamflow, and the duct wall was configured to a No-Slip wall. The turbulent flow at the ducts' inlet and outlet was considered Conservative Interface Flux compared to free streamflow. The pressure boundary conditions were considered at the domain flow's output, and the mean static pressure technique was utilized to modify the local pressure at the boundary. The residual value for the modeled duct's convergence criteria was considered 10^{-4} at the domain setup.

4 Examination Method

This section provides an overview of the equipment and methods of the empirical test of this research. The purpose of the empirical tests is to evaluate and validate the calculations initially. It was then considering the flow intensity inside the duct.

4.1 Inlet Section Pressure Distribution

The static wall pressure was measured in the inlet section. Thirty-seven points perpendicular to the wall were considered to install static pressure ports to measure the pressure distribution in the duct wall, as shown in Figure 6.

Figure 6 - Schematic of the installation of static pressure switches at the inlet contraction wall

A 38-channel pressure distribution system was used to measure the pressure distribution on the model. The primary part of this system is pressure sensors that show voltage changes relative to the pressure applied at the ports (Figure 7). Sensortechnics pressure sensors were used in the measurements, and technical information of sensors is according to Table 1.
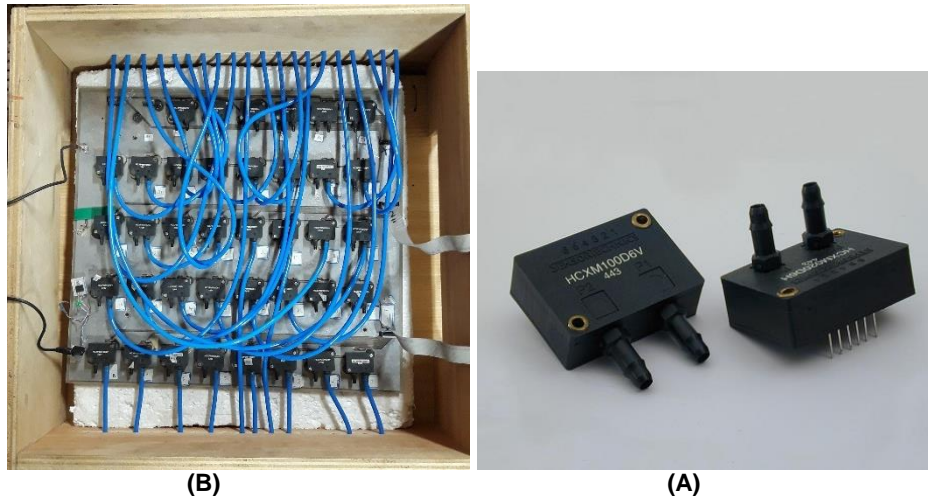
(B)   **(A)**

Figure 7 - Pressure distribution Transducer (A) and measurement system (B)

Table 1 - Specifications of the pressure sensor used in the pressure distribution device

No.	Specification	Description
1	Manufacturer	SENSORTECHNICS
2	Model	HCXPM010D6V
3	Measurement Range	± 10 mbar
4	Sensor Output	Voltage
5	Dimension	39.3 x 35 x 13 mm
6	Input Voltage	15 Volt
7	Type of Inlet	Tube
8	Type of Measurement	Differential, Gauge
9	Min. Working Pressure	-10 °C
10	Max. Working Pressure	+70 °C
11	Output Voltage	5 Volt

The orifices in the contraction section wall were connected to pressure sensors for data collection using pneumatic hoses. The outputs of the pressure sensors were received using the 64-channel terminal and then integrated into the Advantech A/D data card in parallel and using software programed by Tabrizian [43] in the University of Tehran aero lab [43], as shown in Figure 8. Measured pressure was stored as a text file and get ready for analysis. The proprietary software was programmed in the LabView programming environment for reading the pressure distribution in the wall.
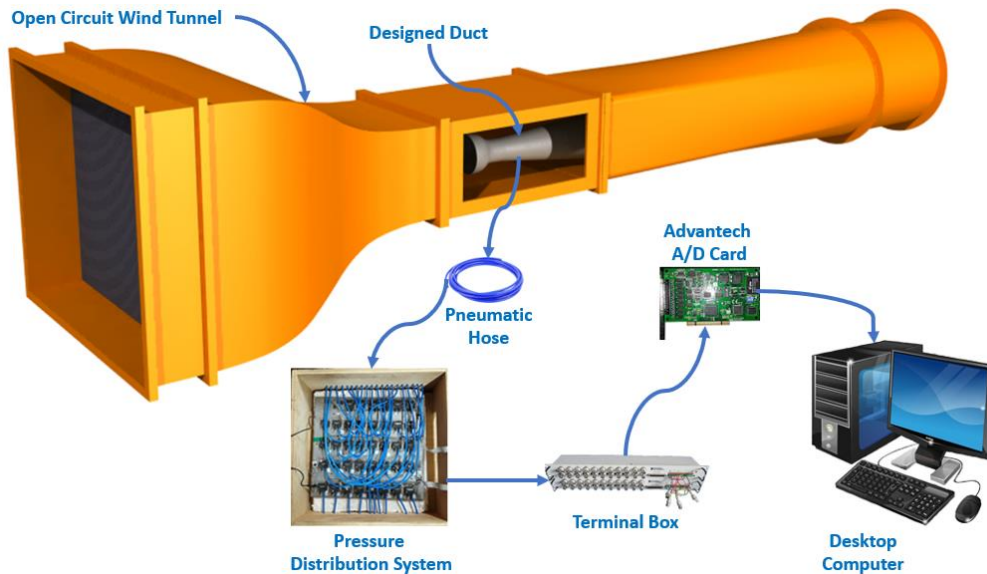
Figure 8 – Arrangement of apparatus used to measure the pressure distribution

4.2 Investigation of speed and turbulence of flow using hot wire sensor

Figure 9 shows the steps of conducting the hot wire anemometer test in the wind tunnel of the University of Tehran Aerospace Faculty. In the first step (1), the hot wire sensor was calibrated relative to the wind tunnel speed. In the second step (2), the hot wire probe was installed inside the duct using two supports; with this regard, that sensor was fixed in the middle of the throat section. The third stage (3) shows the CTA constant temperature anemometer next to the power supply (Manufactured by AEROTECH Gostar CO.). The fourth section (4) illustrates the BNC connection of the cable to transfer data from the sensor probe to the CTA. In section five (5), the data is transmitted online to an A/D card installed on the computer located near the wind tunnel. Finally (6), software designed specifically for this system was used to extract data from an A/D card.

Figure 9- Schematic for Hot-Wire System Arrangement

All experiments in this research were conducted in the wind tunnel of the Experimental Aerodynamics Laboratory of the University of Tehran, Faculty of New Sciences and Technologies. This wind tunnel is an open circuit suction type that includes a bell-shaped inlet, a relaxation chamber with mesh layers, nozzle, test chamber, diffuser, and axial fan. The total length of the tunnel circuit is 12.5 m, and the length of the test section is 1.5 m. Also, its width and height are 1 and 0.7 meters, respectively.

5 Analytical Method

The Analytical Hierarchy Process (AHP) technique is the most frequently used practice to evaluate criteria weights. This method is mathematically authenticated and logically intelligible where all the possible pairs of criteria are compared with each other [45]. The AHP method was applied to data for selecting the best operating condition in the designed ducts. Table 2 presented alternatives and the measured values for them in this study. From these twenty-seven designed ducts, one must choose the best. Three main steps are required to specify the weights of alternatives in the AHP method:

1) Making the hierarchal model decision tree
2) Developing the pairwise comparison judgment matrix and evaluating the priorities
3) Checking consistency of the system

The pairwise comparison matrix $P = (p_{ij})$ is theoretically a ratio of unknown criteria weights: $p_{ij} = w_i/w_j$, $(i, j = 1, 2, . . . , m)$, $p_{ij} = 1/p_{ji}$, $p_{ii} = 1$, where m is the number of criteria. The element pij shows how many times the i-th criterion is more important than the j-th one. The scale 1-3-5-7-9 suggested by the author of the method is applied to the evaluation. The degree of consistency (internal consistency) of the expert evaluations determines the Consistency Index CI and the Consistency Ratio CR:

$$CI = \frac{\lambda_{max} - m}{m - 1} \qquad (5)$$

$$CR = \frac{CI}{RI} \qquad (6)$$

where RI is the average evaluation of CI extracted from simulated matrices with the order of m, acceptable value for the inconsistency of a matrix or a system dependent on the decision-maker, but Saaty [46] indicated 0.1 or below is considered acceptable, and any higher value at any level indicates that the judgments warrant re-examination. The sensitivity analysis confirmed that constant changes in relative weights would prepare proper changes in the final ranking. From sensitivity analysis, it is shown which criterion is the most critical and its

performance measured. The calculation method for sensitivity analysis developed by Godoy and Mangela [47, 48] was used in this study.

Table 2 - Calculated values for inlet contractions with different characteristics

Model	$\tilde{U}$	Θ_w	Θ_v	Separation
1	0.989493	0.000206	0.000283	Yes
2	0.175275	2.08E-05	0.000216	Yes
3	0.710999	6.64E-05	0.001681	Yes
4	0.420176	0.000921	0.000915	Yes
5	0.211377	0.001602	0.000911	Yes
6	0.452231	0.000321	0.000365	Yes
7	0.067092	0.000281	0.000235	No
8	0.184466	0.000114	4.3E-05	No
9	0.098486	0.000805	0.001373	No
10	0.228263	0.000113	0.000152	No
11	0.198692	0.004914	0.00194	Yes
12	0.280703	0.000176	0.000316	Yes
13	0.17721	0.005441	0.001177	Yes
14	0.04906	0.04766	0.001108	Yes
15	0.057836	0.001386	0.007135	Yes
16	0.120212	0.002569	0.001779	No
17	0.132383	0.000326	0.000113	No
18	0.11277	0.000447	0.001785	No
19	0.108259	0.00091	0.000666	No
20	0.268659	0.001387	0.000506	Yes
21	0.184739	0.004414	0.000912	Yes
22	0.066029	0.002809	0.007083	Yes
23	0.072672	0.006367	0.006082	Yes
24	0.080904	0.001019	0.002809	Yes
25	0.130157	0.001362	0.000704	Yes
26	0.132915	0.002949	0.000275	Yes
27	0.127075	0.000186	0.001367	Yes

6   Power Spectral Distribution (PSD)

Spectral analyses are performed to present information about how the signal's energy is distributed concerning frequency. Various techniques for calculating PSD are based on the Fourier Transform provide discrete frequency values inside signal sub-records [49, 50]. Taking the Fourier Transform of a correlation function yields frequency-domain representation in terms of the spectral distribution function, which is equal to energy spectral density in the case of an energy signal [51]. Spectral estimating aims to use a finite amount of data to characterize the distribution (over frequency) of the power contained in a signal. The power spectrum distribution is calculated directly from the signal in our technique and is non-parametric. The spectrum of signals may be estimated using a variety of approaches. A periodogram

approach, which is utilized in this study, is one of these methods. The major benefit of this approach is that the power spectrum distribution (PSD) is directly calculated from the signal [52]. The power spectrum of a signal or process is calculated using this approach by taking the magnitude squared of the discrete-time Fourier transform of the process's samples (typically done on a grid with FFT). The PSD of a signal $x_L[n]$ with a length of L is estimated using a periodogram as follows [53]:

$$P_{xx}(f) = \frac{|x_L(f)|^2}{f_1 L} \qquad (7)$$

$$x_L(f) = \sum_{k=0}^{n-1} x_L[n] \, exp\left(-2\pi i \frac{mk}{n}\right), \quad m = 0, 1, 2, \dots N-1 \qquad (8)$$

where f_1 is the signal's sampling frequency, which in our experiment is equal to 1200, the FFT is generally used to compute $x_L[n]$ since it can only be done at a finite number of frequency points, n. The power contained in a signal will be discussed in this paper by comparing the power spectrum of the signals at various wind velocities, 6, 10, and 14 (m/s).

7 Result & Discussions

Based on the introduced specification in this paper's design section, a 3-D model of ducts was designed (CAD) by Catia V5 R21 software. 3-D models transferred to Ansys workbench to consider engineering parameters (CAE). We have proceeded considerably to prove our design by solving the steady, turbulent, 3-D, Navier Stokes equation inside the duct sections. An unstructured mesh with over 1,000,000 triangular elements was used to mesh the duct sections. A uniform inlet velocity of 10 m/s was defined at the inlet contraction entrance, and a pressure boundary condition was applied at the exit. All of the walls are defined as no-slip wall boundary conditions. Numerical simulation in Ansys CFX was done where a Shear Stress Transport (SST) turbulence model was used to analyze the flow through the duct sections. Ansys CFD-Post was used to extract the results from simulations.

Based on the simulations and analyses results, there is a need for a method to select the best contraction inlet due to the complexity of the calculated indices. Analytical Hierarchy Process (AHP) was used for this purpose; several researchers used this method to select the best alternatives in different designs [47, 54, 55]. 27 No's different contraction models were simulated for the duct, and four criteria of θ_w, θ_v, $\tilde{u}$, and separation in the duct wall were calculated for each model. The analyzes were performed in three stages: (1) hierarchical structure, (2) weighting calculation, and (3) consistency analysis.

7.1 Selecting the Best Inlet Contraction Section

The first step in the hierarchical analysis is to create a graphical representation of the problem. Figure 10 shows the hierarchical choice of the appropriate alternative (best inlet contraction). Level 1 in the hierarchy depicts the goal of selecting the best inlet contraction for the designed duct. In the second level, four criteria of θ_w, θ_v, $\tilde{u}$, and separation are shown, and in the last level of the hierarchy, 27 alternatives are shown.
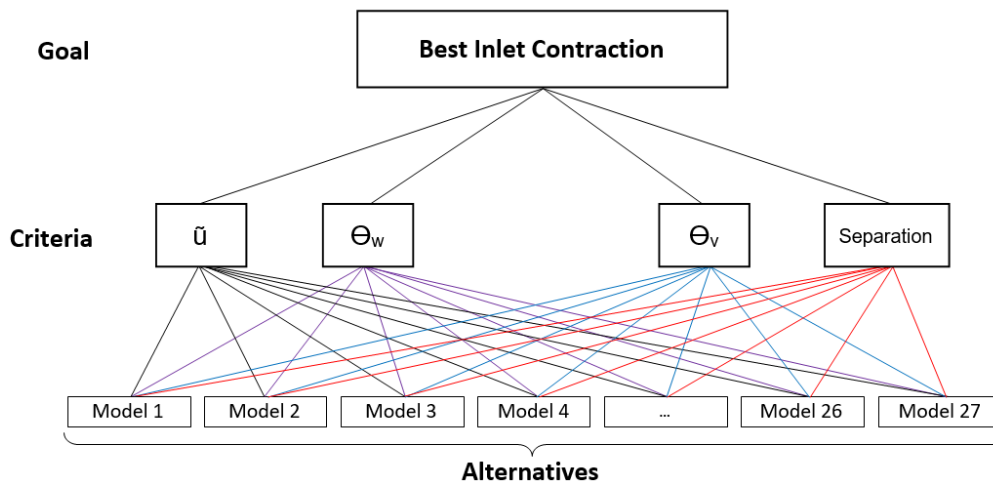

Figure 10. AHP hierarchy for choosing the Best Inlet Contraction

Table 2 shows the calculated values for the various parameters in the inlet contraction section with different specifications that have been introduced previously; these values were used as the main criteria of each designed duct during the analytical hierarchical process.

7.1.1 Calculate the weight to select the best Inlet Contraction section

All comparisons in AHP are made in a pairwise model. For example, suppose the alternatives are compared in flow non-uniformity, first of all. In that case, the first alternative is compared with alternatives two to twenty-seven. Then the comparison would be made for alternative two compared to alternative one and alternatives three to twenty-seven.

Due to the very high importance of separation in the duct wall compared to velocity in the direction of v and w, the preference of velocity index in the direction of v and w were two, and the ratio of separation to non-uniformity of flow was considered 0.33. Table 3 shows the pairwise comparison matrix of criteria. Since the measured values are not the same for different criteria, so the data were validated with numbers on a scale of 1 to 9, such that for the highest wind flow angle in v direction, the number is 1, and with decreasing the angle, the alternatives had a higher index.

Table 3 - Pairwise comparison matrix of criteria

	$\tilde{u}$	Θ_v	Θ_w	Separation
$\tilde{u}$	1	2	2	0.33
Θ_v	0.5	1	1	0.1
Θ_w	0.5	1	1	0.1
Separation	3	10	10	1
Sum	5	14	14	1.53

The pairwise comparisons matrix for flow uniformity, velocity index in the v and w direction, and separation have been done (due to large sizes, tables were not presented in this paper). Also, the normalized matrix and the relative weight calculations of the treatments for the criteria $\tilde{u}$, Θ_v, Θ_w, and separation were calculated.

Arithmetic means the method used to calculate the weight of each alternative in the paired comparison matrix. Since the weight of criteria indicates their importance in the goal, each alternative's weight related to the criteria is the relevant criterion's quota. Then, the final weight for alternatives is obtained by multiplying the weight of each criterion by the weight of its corresponding alternative.

As shown in Table 4, the duct number eight with outlet diameter (D_e) of 0.16m, length of inlet contraction 1.5 times of D_e (0.24m), contraction ratio of three, and blocking ratio of 8.5% was introduced as the best inlet section. After that, ducts seven and ten are shown as the best inlet section. Figure 11 shows a schematic view of the duct wall selected as the best inlet section.

Table 4 - Weights of alternatives in each criterion and final weight of each criterion (W_t) for selecting the best inlet contraction section

No.	$W\,(\ddot{u})$	$W\,(\Theta_v)$	$W\,(\Theta_w)$	$W\,(S)$	W_t
1	0.00093	0.003824	0.004054	0.001932	0.010739
2	0.00651	0.003824	0.005212	0.001932	0.017477
3	0.00279	0.002731	0.005212	0.001932	0.012664
4	0.00465	0.002731	0.002895	0.001932	0.012208
5	0.00651	0.002731	0.001737	0.001932	0.01291
6	0.00465	0.003824	0.004054	0.001932	0.014459
7	0.00837	0.003824	0.004054	0.017384	0.033631
8	0.00651	0.004916	0.005212	0.017384	0.034021
9	0.00837	0.002731	0.002895	0.017384	0.03138
10	0.00651	0.003824	0.005212	0.017384	0.032929
11	0.00651	0.002731	0.000579	0.001932	0.011752
12	0.00651	0.003824	0.005212	0.001932	0.017477
13	0.00651	0.002731	0.000579	0.001932	0.011752
14	0.00837	0.002731	0.000579	0.001932	0.013612
15	0.00837	0.000546	0.001737	0.001932	0.012585

No.	W (ü)	W (Θv)	W (Θw)	W (S)	Wt
16	0.00651	0.002731	0.001737	0.017384	0.028362
17	0.00651	0.003824	0.004054	0.017384	0.031771
18	0.00651	0.002731	0.004054	0.017384	0.030678
19	0.00651	0.002731	0.002895	0.017384	0.02952
20	0.00651	0.002731	0.001737	0.001932	0.01291
21	0.00651	0.002731	0.000579	0.001932	0.011752
22	0.00837	0.000546	0.001737	0.001932	0.012585
23	0.00837	0.000546	0.000579	0.001932	0.011427
24	0.00837	0.001639	0.001737	0.001932	0.013677
25	0.00651	0.002731	0.001737	0.001932	0.01291
26	0.00651	0.003824	0.001737	0.001932	0.014002
27	0.00651	0.002731	0.005212	0.001932	0.016384
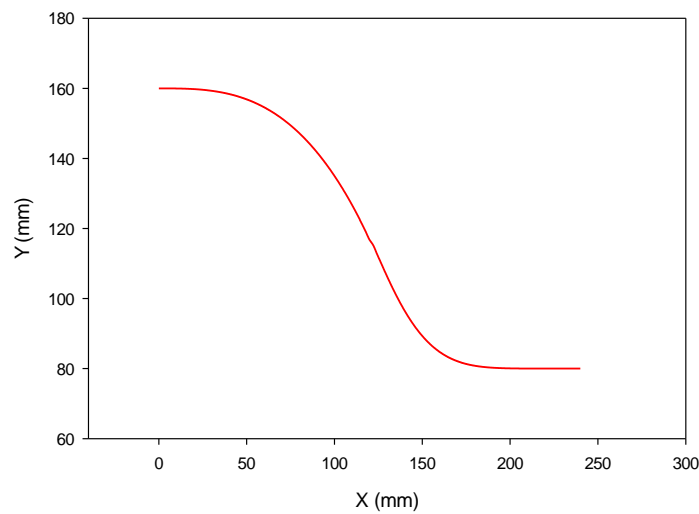
Figure 11 - Schematic of the inlet contraction wall curve at the selected best inlet section

The AHP compatibility is 0.012, which is less than 0.1, and there is no need to reconsider judgments [46]. A set of sensitivity analyzes was performed to evaluate the effect of changes in criteria weighting on the ranking of alternatives [48]. By examining the effect of significant change on the four main criteria on the final results, it was found that alternatives ranking is not sensitive to changes in the importance of the advantage criteria. Figure 12 shows the sensitivity analysis for the four criteria used in this section.

Values of preference weights for listed parameters
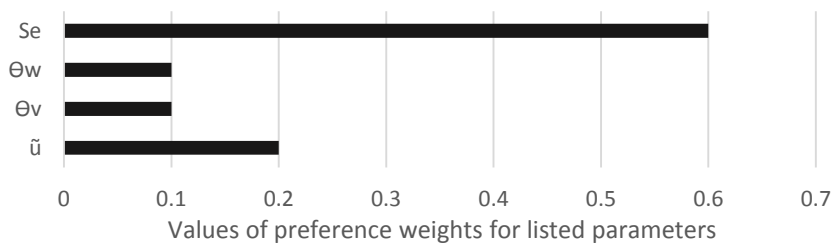
Figure 12 - Sensitivity analysis for four different criteria used

7.2 Selecting the Best Throat Section

Three values of 0.25, 0.75, and 1.5 times the diameter of the duct throat were used to calculate the optimum length of the duct throat section. Figure 13 shows the hierarchical structure to the choice of the best throat section.

Level 1 in the hierarchy shows the goal of selecting the best throat section for the designed duct. In the second level, four criteria θ_w, θ_v, $\tilde{u}$, and separation are shown, and in the last level of the hierarchy, three alternatives (modeled throats) are shown.
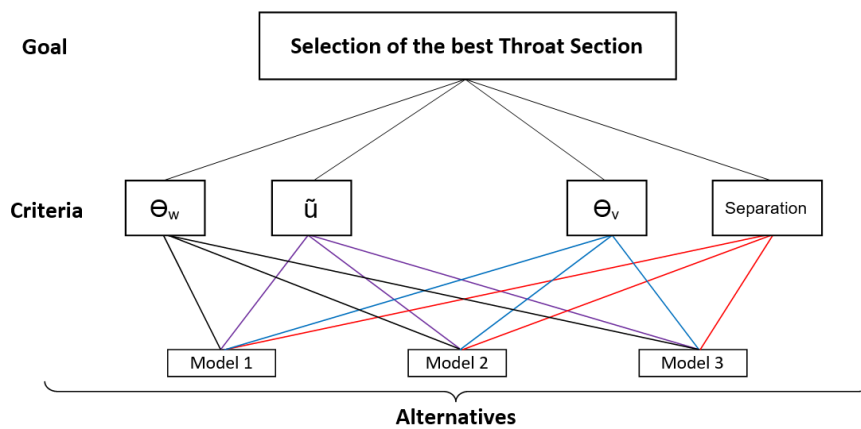
Figure 13. AHP hierarchy for choosing the Best Throat Section

Table 5 shows the values calculated for the various parameters in the three designed throat section models that have been introduced previously.

Table 5 - Calculated values for throat section with different characteristics

Model	$\tilde{u}$	θ_w	θ_v	Separation
1	0.232	0.001439	0.000102	No
2	0.279	0.000401	0.000204	Yes
3	0.321	4.02×10^{-5}	5.11×10^{-6}	No

After calculating the weight of each alternative from the paired comparison matrix (relative weight) by the arithmetic mean method, the weights of the criteria relative to the goal were determined according to the method used to select the best throat section.

Table 6 - Weights of alternatives in each criterion and final weight of each criterion (W_t) for selecting the best throat section

Throat Section	$W(\tilde{u})$	$W(\theta_v)$	$W(\theta_w)$	$W(S)$	W_t
1	0.07533	0.02344	0.01834	0.08326	0.20037
2	0.05859	0.02344	0.02567	0.00925	0.11695
3	0.04185	0.03014	0.03301	0.08326	0.18825

As shown in Table 6, throat section 1 with a length of 0.25 times of throat diameter (0.04 m) is the best throat section for designed ducts. Also, the AHP compatibility is 0.012, which is less than 0.1, and there is no need to reconsider judgments.

7.3 Selecting the best divergence diffuser

Figure 14 shows the hierarchical selection of the best divergent diffuser. Level 1 in the hierarchy shows the goal of selecting the best diffuser for the designed duct. Selecting the best design parameters for the duct diffusers with four criteria, the difference between the ducts was meager, was complicated; therefore, the measured average wind speed at the duct throat section was considered as an additional criterion to decision making analysis to make a difference between the ducts more clear. In the second level, five criteria θ_w, θ_v, $\tilde{u}$, u_{avr}, and separation are shown, and in the last level of the hierarchy, nine alternatives (modeled diffusers) are shown. Also, Table 7 shows the calculated values for five criteria by Ansys CFX for the various nine designed diffusers in the throat sections.
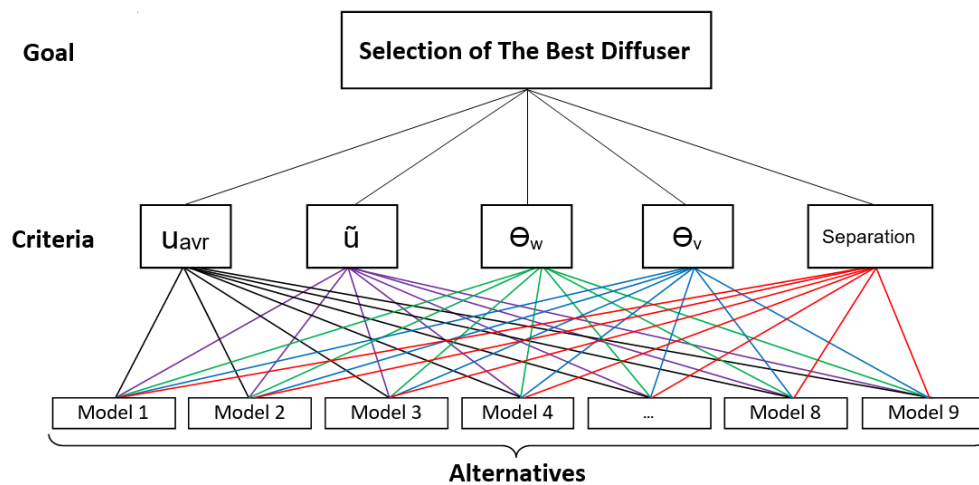

Figure 14 - AHP hierarchy for choosing the Best Diffuser Section

Table 7 - Calculated values for diffuser section with different characteristics

Model	u_{avr}	$\tilde{u}$	θ_w	θ_v	Separation
1	22.8712	0.229643	0.00016	0.000197	Yes
2	23.5724	0.230278	0.000158	4.01E-05	Yes
3	24.0082	0.233853	5.21E-05	3.32E-05	No
4	22.8218	0.230928	0.000519	0.000483	Yes
5	23.7989	0.229738	5.79E-05	0.000227	Yes
6	24.4155	0.234613	7.39E-05	3.83E-05	No
7	22.9276	0.23128	6.25E-05	0.000497	Yes
8	23.9638	0.229763	7.11E-05	0.000168	Yes
9	24.7976	0.234531	0.000108	4.43E-05	No

The weight of each criterion concerning the goal was considered for computing the final weight of alternatives; then, the weight of alternatives in related criterion was calculated. Then that is obvious that the overall weight of alternatives reached via the total weight of criteria multiple the weight of alternative in criteria. Finally, the overall weight of each alternative is computed concerning the local weights.

Table 8 - Weights of alternatives in each criterion and final weight of each criterion (W_t) for selecting the best diffuser section

Model	$W(u_{avr})$	$W(\ddot{u})$	$W(\Theta_v)$	$W(\Theta_w)$	$W(S)$	W_t
1	0.002997	0.009728	0.003943	0.00431	0.003361	0.024339
2	0.008992	0.013619	0.007097	0.00431	0.003361	0.037379
3	0.014987	0.013619	0.007097	0.00554	0.030246	0.07149
4	0.002997	0.013619	0.002366	0.00308	0.003361	0.025422
5	0.014987	0.009728	0.003943	0.00554	0.003361	0.03756
6	0.020981	0.013619	0.007097	0.00554	0.030246	0.077485
7	0.002997	0.013619	0.002366	0.00554	0.003361	0.027885
8	0.014987	0.009728	0.003943	0.00554	0.003361	0.03756
9	0.026976	0.013619	0.007097	0.00554	0.030246	0.08348

As shown in Table 8, diffuser No. 9 is selected as the best diffuser with an outlet angle of 6 degrees relative to the horizontal axis and expansion ratio of 4, and an approximate length of 4.75 times of duct throat diameter (0.76 m). As the calculated consistency index is equal to 0.009398 and is lower than 0.1, the results in Table 8 are acceptable, and there is no need to revise them.

7.4 Investigation of Pressure Distribution in Contraction Inlet

Static pressure was measured along the contraction inlet wall to ensure its effect on the airflow. Thirty-three needles were placed perpendicular to the wall and along with it to measure the static pressure and compare it with the potential flow analysis used in the design of the contraction section,

The distribution of the measured pressure coefficient ($C_p = (P-P_\infty)/0.5\rho U_\infty^2$) is compared with the calculated flow potential in Ansys CFX and shown in Figure 15 and Figure 16. In these graphs, the axial length X is dimensionless with contraction section length L (0.24 m).

Measurements were made at wind speeds of 10 m/s and 14 m/s within the wind tunnel test section (results for 6 m/s not included because of similarity to 10 and 14 m/s curves). The difference between the measured values and the calculated values is minimal. The measured values are slightly higher than the calculated values, while a good match between the two curves is seen (error bars in five-point extracted to check the error of measurements). Error analysis shows that the response received in the practical tests is approximately consistent

with the data calculated in the CFD studies. The general shape of the pressure distribution curve combined with the Stratford criterion [37] shows that the flow separation does not occur along the duct wall.
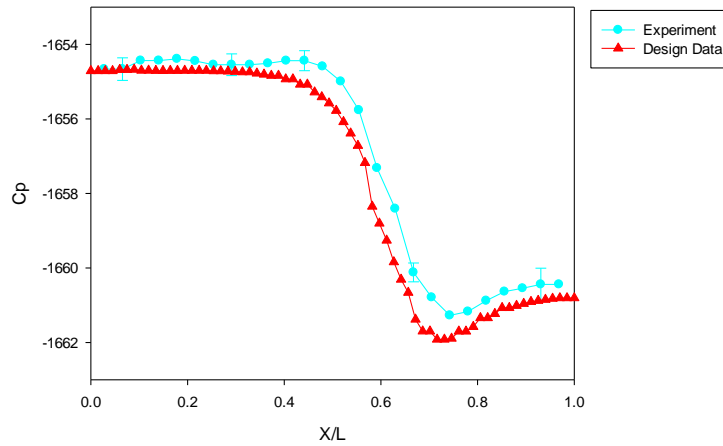

Figure 15 - Comparison of pressure distribution results in the duct wall between the calculated and measured values at 10 m/s.
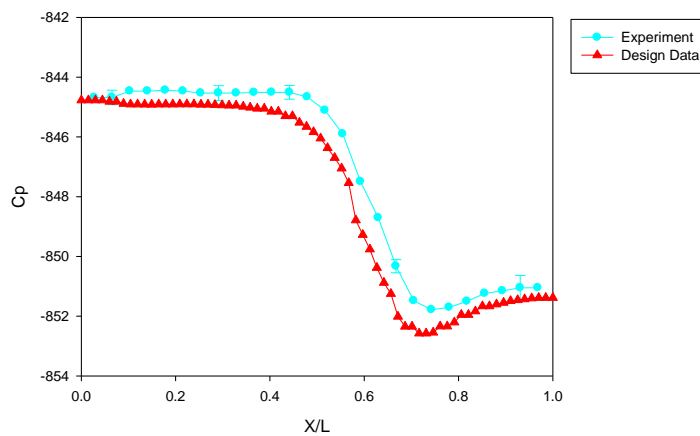

Figure 16 - Comparison of pressure distribution results in the duct wall between the calculated and measured values at 14 m/s.

7.5 Investigation of flow turbulence in the throat section

After extracting the hot wire sensor calibration equation, this equipment was inserted into the throat section to investigate the flow turbulence. Figure 17 shows the voltage changes of the hot wire installed in the throat section of the duct at a velocity of 10 *m/s,* while the setup is located in the wind tunnel.
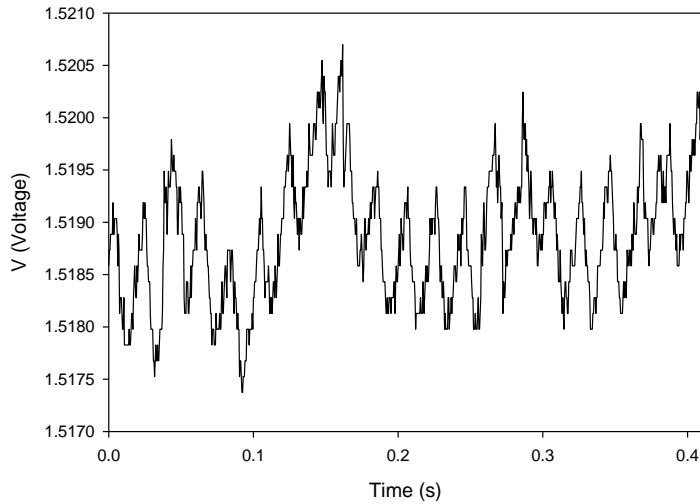
Figure 17 - Measured time data at 10 m/s free flow rate

For better comparison, the measured velocity at the throat section of the duct and the measured velocity within the wind tunnel test section was plotted against the velocity index of the wind tunnel test section (Figure 18). The first-order equation line is plotted via the measured points (the coefficient of determination, R^2, is above 0.99). As can be seen, the increment of the velocity at the duct throat section is much higher than the velocity increment at the wind tunnel. From the plotted line, it can be concluded that the velocity within the duct increases at a constant ratio.
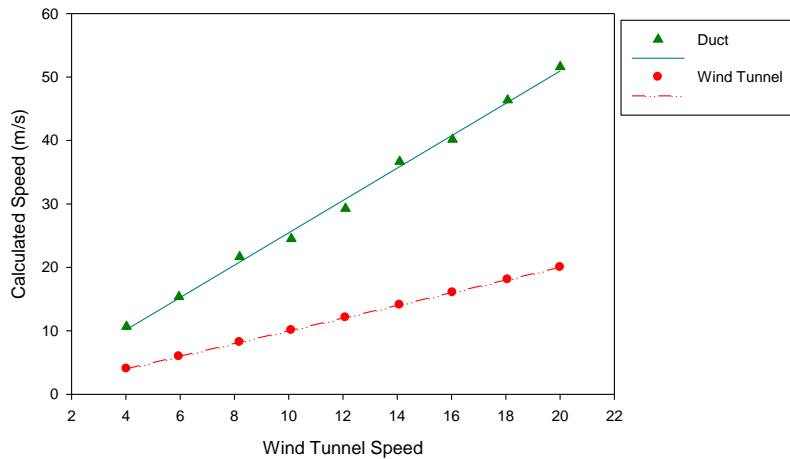
Figure 18 - Comparison of wind tunnel velocity and duct throat section velocity at different wind speeds

To investigate the increment rate of wind velocity inside the throat section compared to the flow speed in the wind tunnel plotted as a bar chart at different wind speeds in the tunnel. Figure 19 shows that at different wind speeds, the increase in velocity due to the inlet contraction is a velocity ratio between 2.6 and 2.9. As calculated by Bontempo [56], the maximum available wind power for each general wind turbine can be calculated by:

$$P_a = \frac{16}{27} \rho A v^3 \qquad\qquad (9)$$

where ρ is the air density, A is the swept area of turbine, and v is the wind speed. Then we can compare the available power for a wind turbine installed in the inlet section, complete with related area and wind speed in this section, with another wind turbine installed in the throat section of the duct. To show the efficiency of the designed duct via Eq. (9), we know the contraction ratio is 0.333, and the minimum wind speed increment is 2.6. We found the available power in the throat section increased about 5.85 times compared to the traditional turbine with the diameter of the inlet section of the duct. Allaei [8] reported, the average power output in CFD analysis on Invelox was increased five times. However, as we know, the Invelox has a large entrance and a long tower to capture the wind compared to the designed duct in this paper. Compared to traditional wind turbine power, the designed duct can introduce 85% more available wind power than Invelox even though the operation of conventional wind turbines will be halted if the wind speed is greater than the cut-out speed (typically about 25 *m/s*) to prevent turbine failures caused by strong loads applied to the turbines. But in ducted wind turbines, we can extend the cut speed range, including both cut-in and cut-out speeds, because of size reduction.
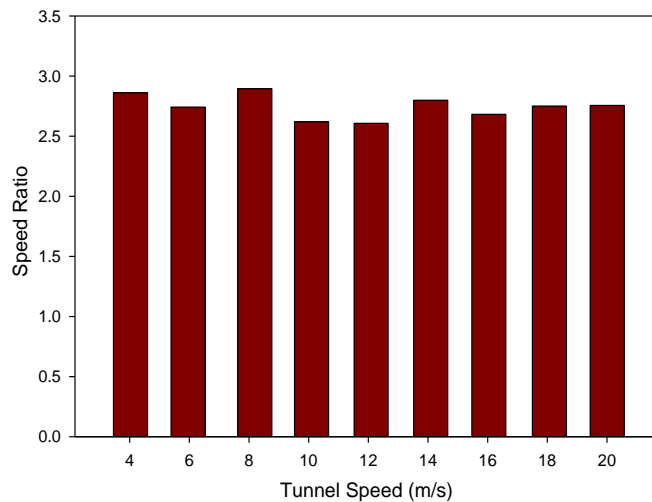

Figure 19 - The ratio of the velocity in the throat section to the wind tunnel speed at different speeds

As shown in Figure 17, we need to extract wind speed from the measured signal. Then before analyzing the signal, we checked the normal distribution to make sure that signal quality was confirmed. Then the distribution of output signals from hot-wire sensors is considered. The deviation from the Gaussian distribution function can be investigated using skewness and kurtosis because the relationship between the number of degrees of freedom in space and time decreases locally. Skewness is a criterion for examining symmetry, or more precisely,

asymmetry of data. Kurtosis or flatness is a parameter that indicates measured data is more or less sharp than the normal distribution at the maximum sharp point.

Figure 20 shows the skewness and kurtosis changes, respectively, at different wind velocities across the duct throat section. The skewness for the normal distribution is zero, and any symmetric skewness data is close to zero. The plotted line in Figure 20 (A) shows that the absolute value of skewness for all velocities is very close to zero. This means that there is no significant violation in assuming the extracted data form a normal distribution. The measured skewness represents both negative and positive values, which means that the skewness of the data is close to the normal distribution.

(A)   (B)
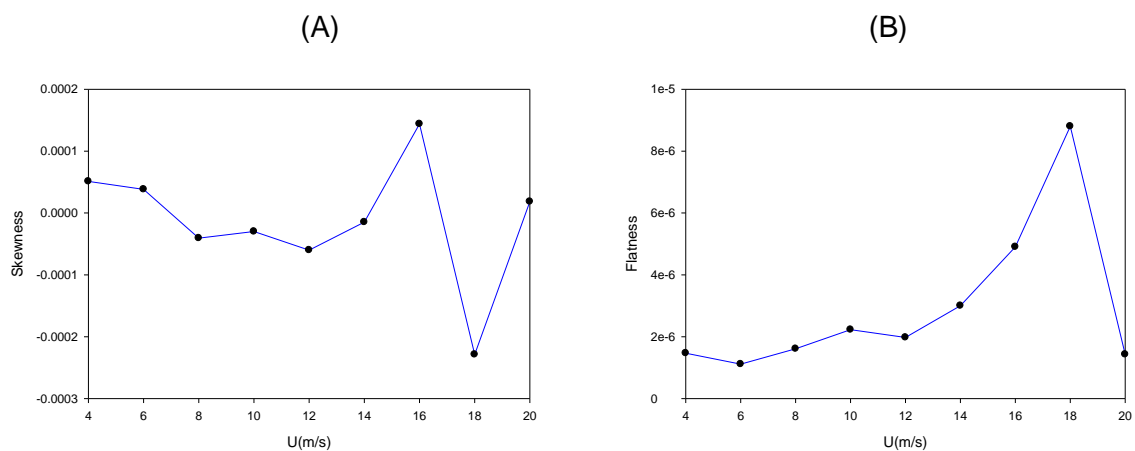
Figure 20 – Skewness (A) and Kurtosis changes at different wind velocities at throat cross-section

Figure 20 (B) shows the amount of kurtosis or flatness for the signals at all throat cross-section velocities. Flatness measured the tail weight (standard distribution peak point) to the sharpness of the distribution. Positive kurtosis indicates peak distribution more than the normal distribution, and negative kurtosis indicates smooth distribution near to normal pattern. Figure 20 (B) shows that these data have heavy-tailed distributions.

Figure 21 shows the turbulence intensity at the duct throat section at different wind tunnel velocities; according to Bardal & Sætran's [57] research, the turbulence intensity above 10% significantly reduced the wind turbine output power. As can be seen, the measured values for turbulence intensity at all wind speeds of 4-20 *m/s* are a maximum of 0.65%, which is far below 10% and does not disturb the performance of the wind turbine installed at the throat section.
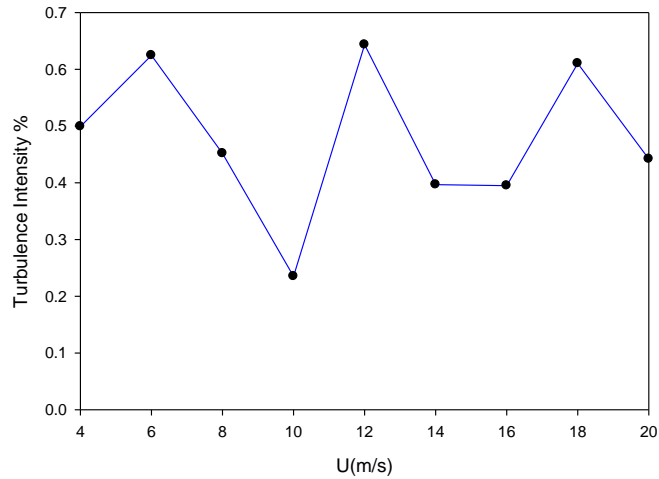
Figure 21 - Turbulence Intensity of throat sections at different wind tunnel speeds

7.6 Spectral analysis of the flow velocity

Fast Fourier transform and power spectrum distribution were performed to investigate the content of the airflow rate signal. A hot wire sensor was placed in the center of the duct throat section to measure the velocity signal. Fast Fourier transform is used to measure the frequency content of fixed or transient signals and simulate the signal's mean frequency content at all data points. The power spectrum distribution was calculated and plotted to investigate the energy content of the signal. Figure 22 shows the power spectrum distribution at speeds of 6 *m/s*, 10 *m/s*, and 14 *m/s*.
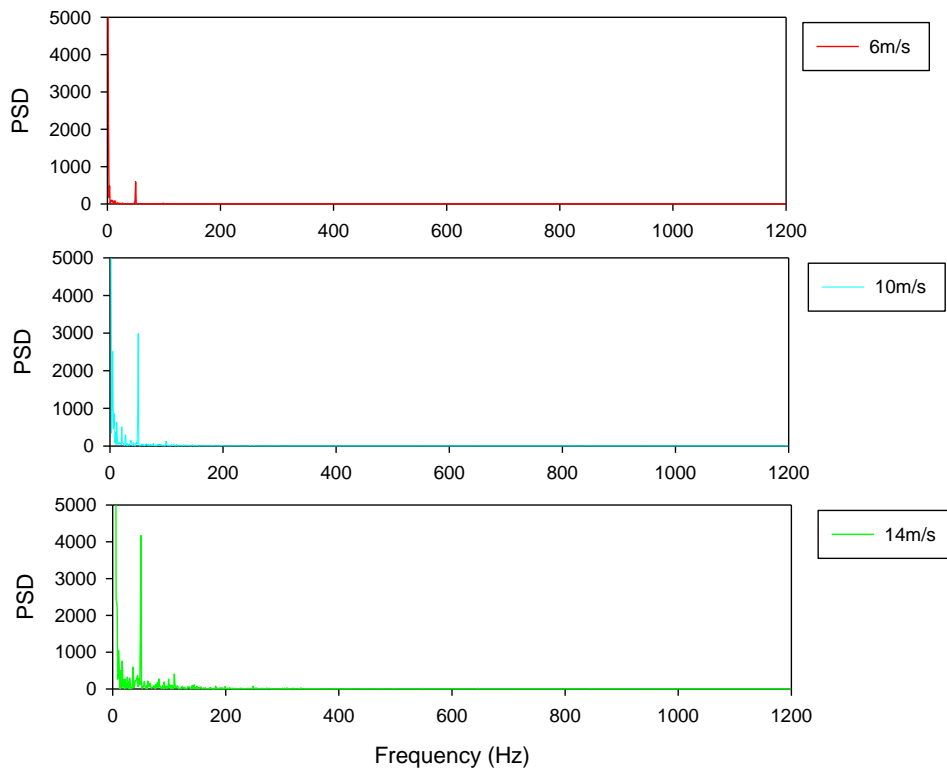
Figure 22 - PSD of the velocity signal at throat section at different wind tunnel flow rate

Obviously, by decreasing the flow rate at the duct inlet, the power spectrum amplitude decreases, indicating a decrease in the flow energy content at all frequencies.

Two prominent peaks are shown in Figure 22, during the tests the duct located inside the wind tunnel and is mounted on the floor of the wind tunnel test section. The vibrations of the tunnel wall affect the duct, and the low-frequency peak can be attributed to these vibrations. The second peak occurred at a frequency of 32 *Hz* due to the instabilities associated with the wind flow contraction at the inlet and the Gartler vortex at the turning point of the contraction section [58]. These frequencies indicate instability in the boundary layer of the duct wall, which is one of the factors affecting the intensity of turbulence in the duct. The absence of more peaks or lower altitudes of higher frequencies indicates a low degree of turbulence within the duct. It can be said that it will not significantly impact the performance of the wind turbine placed inside the duct.

8 Conclusion

In this paper, a parametric study on the convergent-divergent duct was conducted to determine the optimized dimensions of the duct. Then a prototype of the duct was fabricated, and experimental tests were performed to validate the analysis. Both modeling and

experimental sections reached good results. The optimized duct design was performed step by step. Initially, the inlet contraction was modeled and simulated using Catia V5 and ANSYS CFX engineering analysis software, Respectively. The 27-line equations were designed for the contraction crater wall, and the variables θ_w, θ_v, $\tilde{u}$, and separation along the wall were calculated. AHP was used to select the best duct inlet contraction with outlet diameter (D_e) of 0.16 m, length of inlet contraction (L) 1.5 times of D_e (0.24 m), contraction ratio (CR) of 3, and blocking ratio (BR) of 8.5%.

The length of the throat was evaluated to select the best throat section. AHP was used, and the throat length equal to 0.25 times of throat diameter (D_e) was selected as the best throat section. The pressure recovery in the divergent diffuser is independent of the shape of the wall. The diffuser with a 15% expanding ratio and an approximate length of 4.75 times of throat diameter is selected as the best diffuser. The pressure distribution in the inlet contraction wall of the duct showed that the difference between the measured and calculated values was minimal, the total error was determined, and a good adoption was observed between the two values. Examination of the inlet contraction's pressure distribution showed no significant inverse pressure gradient at the inlet section. Therefore no separation occurred in the inlet contraction nozzle. Flow intensity at the throat section was investigated using a hot wire sensor. The velocity measurements showed between 2.6 and 2.9 times the channel cross-section relative to the free flow. The measured turbulence intensity shows values near zero (maximum of 0.65%) at different velocities from 2 m/s to 20 m/s; this variable indicates the uniformity of the flow inserted to the contraction input and delivered to the duct throat section. The frequency content of the measured signals was investigated by using the Fast Fourier Transform. It was shown that the energy level decreased at all frequencies with decreasing wind speed in free-stream flow. Examination of the power spectrum distribution revealed a few peaks are indicating low turbulence inside the duct, and it can be concluded that the flow disturbances do not have a significant impact on the performance of the wind turbine placed inside the duct throat. The optimized duct can be used as an energy conversion system in new ducted wind turbines like Invelox, Zena, Airborn, etc.

9   References

1.   Wang, W.C., Wang, J.J., Chong, W.T.: The effects of unsteady wind on the performances of a newly developed cross-axis wind turbine: A wind tunnel study. Renewable Energy. 131, 644–659 (2019). https://doi.org/10.1016/j.renene.2018.07.061

2. Kumar, V., Saha, S.: Theoretical performance estimation of shrouded-twin-rotor wind turbines using the actuator disk theory. Renewable Energy. 134, 961–969 (2019). https://doi.org/10.1016/j.renene.2018.11.077

3. Riyanto, Pambudi, N.A., Febriyanto, R., Wibowo, K.M., Setyawan, N.D., Wardani, N.S., Saw, L.H., Rudiyanto, B.: The performance of shrouded wind turbine at low wind speed condition. Energy Procedia. 158, 260–265 (2019). https://doi.org/10.1016/j.egypro.2019.01.086

4. Allaei, D., Tarnowski, D., Andreopoulos, Y.: INVELOX with multiple wind turbine generator systems. Energy. 93, 1030–1040 (2015). https://doi.org/10.1016/j.energy.2015.09.076

5. Wong, L.: A Review of Transmission Losses in Planning Studies. California Energy Commission. CEC- 200, (2011)

6. Dannecker, R.K.W., Grant, A.D.: Investigations of a building-integrated ducted wind turbine module. Wind Energy. 5, 53–71 (2002). https://doi.org/10.1002/we.60

7. Taghinezhad, J., Alimardani, R., Masdari, M., Mahmoodi, E.: Performance optimization of a dual-rotor ducted wind turbine by using response surface method. Energy Conversion and Management: X. 12, 100120 (2021). https://doi.org/10.1016/j.ecmx.2021.100120

8. Allaei, D.: Using CFD to Predict the Performance of Innovative Wind Power Generators. In: Proceedings of the 2012 COMCOL Conference. pp. 2–3 (2012)

9. Allaei, D., Andreopoulos, Y.: INVELOX: A new concept in wind energy harvesting. In: ASME 2013 7th International Conference on Energy Sustainability. pp. 1–5 (2013)

10. Allaei, D., Andreopoulos, Y.: INVELOX: Description of a new concept in wind power and its performance evaluation. Energy. 69, 336–344 (2014). https://doi.org/10.1016/j.energy.2014.03.021

11. Anbarsooz, M., Hesam, M.S., Moetakef-Imani, B.: Numerical study on the geometrical parameters affecting the aerodynamic performance of Invelox. IET Renewable Power Generation. 11, 791–798 (2017). https://doi.org/10.1049/iet-rpg.2016.0668

12. Anbarsooz, M., Amiri, M., Rashidi, I.: A novel curtain design to enhance the aerodynamic performance of Invelox: A steady-RANS numerical simulation. Energy. 168, 207–221 (2019). https://doi.org/10.1016/j.energy.2018.11.122

13. Han, W., Yan, P., Han, W., He, Y.: Design of wind turbines with shroud and lobed ejectors for efficient utilization of low-grade wind energy. Energy. 89, 687–701 (2015). https://doi.org/10.1016/j.energy.2015.06.024

14. Bontempo, R., Manna, M.: Performance analysis of open and ducted wind turbines. Applied Energy. 136, 405–416 (2014). https://doi.org/10.1016/j.apenergy.2014.09.036

15. Bagheri-Sadeghi, N., Helenbrook, B.T., Visser, K.D.: Ducted wind turbine optimization and sensitivity to rotor position. Wind Energy Science. 3, 221–229 (2018). https://doi.org/10.5194/wes-3-221-2018

16. Wibowo, T.T., Daulay, F.H., Suryopratomo, K., Budiarto, R.: Numerical study of the effect of geometry variation on the performance of innovative design wind speed enhancer. In: E3S Web of Conferences. p. 01013. EDP Sciences (2018)

17. Chaudhari, C.D., Waghmare, S.A., Kotwal, A.: Numerical Analysis of Venturi Ducted Horizontal Axis Wind Turbine for Efficient Power Generation Numerical Analysis of Venturi Ducted Horizontal Axis Wind Turbine for Efficient Power Generation. International Journal of Mechanical Engineering and Computer Applications. 1, 90–93 (2013)

18. Agha, A., Chaudhry, H.N., Wang, F.: Determining the augmentation ratio and response behaviour of a Diffuser Augmented Wind Turbine (DAWT). Sustainable Energy Technologies and Assessments. 37, 100610 (2020). https://doi.org/10.1016/j.seta.2019.100610

19. Ehsan, M.M., Ovy, E.G., Chowdhury, H.A., Ferdous, S.M.: A Proposal of implementation of ducted wind turbine integrated with solar system for reliable power generation in Bangladesh. International Journal of Renewable Energy Research. 2, 397–403 (2012). https://doi.org/10.20508/ijrer.36008

20. Kanya, B., Visser, K.D.: Experimental Validation of a Ducted Wind Turbine Design Strategy. Wind Energy Science Discussions. 1–22 (2017). https://doi.org/10.5194/wes-2017-54

21. Masukume, P.-M., Makaka, G., Tinarwo, D.: Technoeconomic Analysis of Ducted Wind Turbines and Their Slow Acceptance on the Market. Journal of Renewable Energy. 2014, 1–5 (2014). https://doi.org/10.1155/2014/951379

22. Taghinezhad, J., Alimardani, R., Mosazadeh, H., Masdari, M.: Ducted Wind Turbines A Review. International Journal on Future Revolution in Computer Science & Communication Engineering. 5, 19–25 (2019)

23. Solangi, Y.A., Tan, Q., Khan, M.W.A., Mirjat, N.H., Ahmed, I.: The selection of wind power project location in the Southeastern Corridor of Pakistan: A factor analysis, AHP, and fuzzy-TOPSIS application. Energies. 11, (2018). https://doi.org/10.3390/en11081940

24. Dinmohammadi, A., Shafiee, M.: Determination of the most suitable technology transfer strategy for wind turbines using an integrated AHP-TOPSIS decision model. Energies. 10, (2017). https://doi.org/10.3390/en10050642

25. Konstantinos, I., Georgios, T., Garyfalos, A.: A Decision Support System methodology for selecting wind farm installation locations using AHP and TOPSIS: Case study in Eastern Macedonia and Thrace region, Greece. Energy Policy. 132, 232–246 (2019). https://doi.org/10.1016/j.enpol.2019.05.020

26. Mathew, J., Bahr, C., Carroll, B., Sheplak, M., Cattafesta, L.: Design, fabrication, and characterization of an anechoic wind tunnel facility. Collection of Technical Papers - 11th AIAA/CEAS Aeroacoustics Conference. 5, 3142–3152 (2005). https://doi.org/10.2514/6.2005-3052

27. Morel, T.: Comprehensive Design of Axisymmetric Wind Tunnel Contractions. Journal of Fluids Engineering. 225–233 (1975)

28. Derbunovich, G.I., Zemskaya, A.S., Repik, E.U., Sosedko, Y.P.: Effect of flow contraction on the level of turbulence. Fluid Dynamics. 22, 289–294 (1987). https://doi.org/10.1007/BF01052265

29. Jafari, S.A.H., Kosasih, B.: Flow analysis of shrouded small wind turbine with a simple frustum diffuser with computational fluid dynamics simulations. Journal of Wind Engineering and Industrial Aerodynamics. 125, 102–110 (2014). https://doi.org/10.1016/j.jweia.2013.12.001

30. Vaz, J.R.P., Wood, D.H.: Aerodynamic optimization of the blades of diffuser-augmented wind turbines. Energy Conversion and Management. 123, 35–45 (2016). https://doi.org/10.1016/j.enconman.2016.06.015

31. Shi, L., Feng, F., Guo, W., Li, Y.: Research and Development of a Small-Scale Icing Wind Tunnel Test System for Blade Airfoil Icing Characteristics. International Journal of Rotating Machinery. 2021, 1–12 (2021). https://doi.org/https://doi.org/10.1155/2021/5598859 Research

32. Zanoun, E.S.: Flow characteristics in low-speed wind tunnel contractions: Simulation and testing. Alexandria Engineering Journal. 57, 2265–2277 (2018). https://doi.org/10.1016/j.aej.2017.08.024

33. de Almeida, O., de Miranda, F.C., Ferreira Neto, O., Saad, F.G.: Low subsonic wind tunnel - Design and construction. Journal of Aerospace Technology and Management. 10, 1–20 (2018). https://doi.org/10.5028/jatm.v10.716

34. Sukumar, P.: Parametric Study on Ducted Wind Turbine System and Flow Characteristics When Placed on Top of a Building, (2015)

35. Javaherchi, T., Stelzenmuller, N., Aliseda, A.: Experimental and numerical analysis of the performance and wake of a scale-model horizontal axis marine hydrokinetic turbine. Journal of Renewable and Sustainable Energy. 9, 1–23 (2017). https://doi.org/10.1063/1.4999600

36. Cattafesta, L., Bahr, C., Mathew, J.: Fundamentals of Wind-Tunnel Design. Encyclopedia of Aerospace Engineering. 1–10 (2010). https://doi.org/10.1002/9780470686652.eae532

37. Stratford, B.S.: The prediction of separation of the turbulent boundary layer. Journal of Fluid Mechanics. 5, 1–16 (1959). https://doi.org/10.1017/S0022112059000015

38. Pinto, M.L., Franzini, G.R., Simos, A.N.: A CFD analysis of NREL's 5MW wind turbine in full and model scales. Journal of Ocean Engineering and Marine Energy. 6, 211–220 (2020). https://doi.org/10.1007/s40722-020-00162-y

39. Giahi, M.H., Jafarian Dehkordi, A.: Investigating the influence of dimensional scaling on aerodynamic characteristics of wind turbine using CFD simulation. Renewable Energy. 97, 162–168 (2016). https://doi.org/10.1016/j.renene.2016.05.059

40.   Qader, B.S., Supeni, E.E., Ariffin, M.K.A., Talib, A.R.A.: RSM approach for modeling and optimization of designing parameters for inclined fins of solar air heater. Renewable Energy. 136, 48–68 (2019). https://doi.org/10.1016/j.renene.2018.12.099

41.   Sayed, M.A., Kandil, H.A., Shaltot, A.: Aerodynamic analysis of different wind-turbine-blade profiles using finite-volume method. Energy Conversion and Management. 64, 541–550 (2012). https://doi.org/10.1016/j.enconman.2012.05.030

42.   Rahmannezhad, J., Mirbozorgi, S.A.: CFD analysis and RSM-based design optimization of novel grooved micromixers with obstructions. International Journal of Heat and Mass Transfer. 140, 483–497 (2019). https://doi.org/10.1016/j.ijheatmasstransfer.2019.05.107

43.   Tabrizian, A.: An Experimental Study of the Effects of Sweep Wing on the Boundary Layer of 2D Wing, http://repository.sharif.edu/resource/389977/-/&from=search&&query=swept-wing&field=subjectkeyword&count=20&execute=true, (2013)

44.   Aerodynamic Research Lab., http://aerolab.ut.ac.ir/

45.   Vinogradova- zinkevič, I., Podvezko, V., Zavadskas, E.K.: Comparative assessment of the stability of ahp and fahp methods. Symmetry. 13, (2021). https://doi.org/10.3390/sym13030479

46.   Saaty, T.L.: The Analytic Hierarchy Process: Planning, Priority Setting, Resource Allocation., http://www.oalib.com/references/15389320

47.   Godoy, D.L.P.: Application of the Fuzzy-AHP method in the optimization of production of concrete blocks with addition of casting sand. Journal of Intelligent and Fuzzy Systems. 35, 3477–3491 (2018). https://doi.org/10.3233/JIFS-17729

48.   Kumar, S., Kumar, P., Kumar, M.: Risk analysis in green supply chain using fuzzy AHP approach : A case study. Resources, Conservation and Recycling. 104, 375–390 (2015)

49.   Zhu, B., Shi, Y., Chen, Q., Wang, Y.: Measuring vortex-induced vibration with hot wire in wind tunnel. Proceedings - 2017 4th International Conference on Information Science and Control Engineering, ICISCE 2017. 1534–1538 (2017). https://doi.org/10.1109/ICISCE.2017.320

50. Wittwer, A.R., Dorado, R., Alvarez, G., Degrazia, G.A., Loredo-souza, A.M., Bodmann, B.: Flow in the Wake of Wind Turbines : Turbulence Spectral Analysis by Wind Tunnel Tests. American Journal of Environmental Engineering. 6, 109–115 (2016). https://doi.org/10.5923/s.ajee.201601.16

51. Kramti, S.E., Ali, J. ben, Bechhoefer, E., Takrouni, K., Darghouthi, A., Sayadi, M.: Toward an online strategy for mechanical failures diagnostics inside the wind turbine generators based on spectral analysis. Wind Engineering. 45, 782–792 (2021). https://doi.org/10.1177/0309524X211028759

52. Taghinezhad, J., Mahmoodi, E., Masdari, M., Alimardani, R.: Spectral Analyses of an Optimized Ducted Wind Turbine using Hot-Wire Anemometry. In: 7th Iran Wind Energy Conference (IWEC2021). pp. 1–4. IEEE (2021)

53. Dehghan Manshadi, M., Tamadonfar, P., Soltani, M.R., Ghorbanian, K., Masdari, M.: Power spectrum and FFT-Based signal analysis in turbulence measurements. World Academy of Science, Engineering and Technology. 40, 275–278 (2009)

54. Eroglu, H., Aydin, M.: Optimization of electrical power transmission lines' routing using AHP, fuzzy AHP, and GIS. Turkish Journal of Electrical Engineering and Computer Sciences. 23, 1418–1430 (2015). https://doi.org/10.3906/elk-1211-59

55. Taghinezhad, J., Alimardani, R., Jafari, A.: Optimization cane traction output from hopper in full-automatic sugarcane planters by using response surface modeling and analytical hierarchy process. Agricultural Engineering International: CIGR Journal. 15, 138–147 (2013)

56. Bontempo, R., Carandente, R., Manna, M.: A design of experiment approach as applied to the analysis of diffuser-augmented wind turbines. Energy Conversion and Management. 235, 113924 (2021). https://doi.org/10.1016/j.enconman.2021.113924

57. Bardal, L.M., Sætran, L.R.: Influence of turbulence intensity on wind turbine power curves. Energy Procedia. 137, 553–558 (2017). https://doi.org/10.1016/j.egypro.2017.10.384

58. Unalmis, O.H.: On the possible relationship between low frequency unsteadiness of shock-induced separated flow and Goertler vortices. Fluid Dynamics. (2002). https://doi.org/10.2514/6.1996-2002